

# Real-Time Detection of Unmodeled Gravitational-Wave Transients Using Convolutional Neural Networks

Vasileios Skliris, Michael R. K. Norman, and Patrick J. Sutton

*Gravity Exploration Institute, School of Physics and Astronomy,  
Cardiff University, Cardiff, United Kingdom CF24 3AA*

(Dated: 7. Juni 2022)

Convolutional Neural Networks (CNNs) have demonstrated potential for the real-time analysis of data from gravitational-wave detector networks for the specific case of signals from coalescing compact-object binaries such as black-hole binaries. Unfortunately, training these CNNs requires a precise model of the target signal; they are therefore not applicable to a wide class of potential gravitational-wave sources, such as core-collapse supernovae and long gamma-ray bursts, where unknown physics or computational limitations prevent the development of comprehensive signal models. We demonstrate for the first time a CNN with the ability to detect generic signals – those without a precise model – with sensitivity across a wide parameter space. Our CNN has a novel structure that uses not only the network strain data but also the Pearson cross-correlation between detectors to distinguish correlated gravitational-wave signals from uncorrelated noise transients. We demonstrate the efficacy of our CNN using data from the second LIGO-Virgo observing run, and show that it has sensitivity comparable to that of the “gold-standard” transient searches currently used by LIGO-Virgo, at extremely low (order of 1 second) latency and using only a fraction of the computing power required by existing searches, allowing our models the possibility of true real-time detection of gravitational-wave transients associated with gamma-ray bursts, core-collapse supernovae, and other relativistic astrophysical phenomena.

## I. INTRODUCTION

Gravitational-wave (GW) astronomy is now an established field of observational science. To date, the LIGO [1] and VIRGO[2] collaborations have published the details of 15 high-confidence detections [3–7], and released public alerts for more than 50 additional candidate signals [8]. The detected signals originate from the binary inspiral and merger of two black holes [9], two neutron stars [10], or one object of each type [11].

Low-latency detection of candidate signals offers arguably the greatest potential scientific payoff, as the GW observations can trigger followup observations in other channels; *i.e.*, multi-messenger astronomy. For example, combined GW and electromagnetic observations of GW170817 - GRB 170817A [12] have yielded novel insights into the origin of heavy elements [13], neutron-star structure [14], GRB astrophysics and host environments [15], and the Hubble constant [16]. Electromagnetic followup of gravitational-wave signals requires very low latency analysis of the GW data - preferably at the second scale to capture the highest energy emissions (*e.g.*, the prompt gamma and x-ray emission of GRBs), so that it produces accurate sky localisation results to make the follow up possible. Current GW analysis techniques rely on hundreds to thousands of dedicated CPUs and achieve minute-scale latency [17].

Recent work by a number of authors [18–22] has shown that a fundamentally different approach using convolutional neural networks (CNNs) has the potential to analyse detector data for GW signals in real time ( $\sim 1$ s latency) using a single dedicated GPU. This could reduce the time required to identify candidate GW signals by approximately two orders of magnitude, potentially

revolutionising multi-messenger astronomy with GWs.

To fully explore the new GW window we need to be able to detect signals from the widest possible variety of sources. Many potential sources are governed by physics which is either unknown (*e.g.* the neutron star equation of state) and/or computationally intractable (*e.g.* the modelling of core-collapse supernovae [23] and accretion-disk instabilities [24]); their transient signals are commonly known as gravitational wave bursts (GWBs). While the unknown physics governing GWBs makes the study of such signals exciting, it also poses a challenge: CNNs demonstrated to date are only capable of detecting signals with a precisely defined signal model, compact binary coalescences.

We address this challenge by proposing a novel CNN architecture that analyses not only the detector strain data directly but also the cross-correlation timeseries between detectors. By training the CNN with ‘featureless’ (randomised) signals, we are able to construct a neural network that detects coherence between detectors rather than specific signal shapes in individual detectors. We test the trained CNN with real data from the LIGO-Virgo network and show that it is capable of detecting a variety of simulated GWB signal morphologies without being specifically trained for them, at sensitivities close to that of standard GWB searches, but at much lower latency and a tiny fraction of the computational cost.

## II. METHOD

### A. Network Architecture

Our goal is to be able to detect sub-second-duration GWBs in data from the three detectors of the LIGO-Virgo network, without prior knowledge of the signal morphology. A significant challenge is to distinguish real signals from the background noise transients, “glitches”, that are common in these detectors [25–27].

Typical GWB detection algorithms [28–31] do this by requiring candidate signals to be seen simultaneously in multiple detectors (simultaneously up to the light travel time between the detectors) and to be correlated between detectors. We follow this logic in our analysis by using a network architecture that combines the outputs of two different CNNs: one that detects coincident signals in multiple detectors, and a second that detects correlation between the detectors.

The first CNN, model 1, is a simple single-input single-output sequential case that was adapted from Gabbard *et al.* [19] and then optimised for this specific task using trial and error. Its architecture can be seen in Table I. This model takes as input the whitened timeseries data from each of the three LIGO-Virgo detectors. The output is a score on [0, 1], where high values indicate signal and low values no signal. This CNN is trained to identify transients that are present simultaneously in two or three detectors, and to distinguish them from transients that are present only in one detector (typical of noise).

Hyper Param.		Model 1 Layers							
Layer No.		1	2	3	4	5	6	7	8
Layer Type	C	C	C	C	C	D	D	D	D
Filters	1024	512	256	128	32	128	64	2	
Kernel size	3	3	3	3	3	n/a	n/a	n/a	
MaxPool	n/a	n/a	4	n/a	4	n/a	n/a	n/a	
DropOut	n/a	n/a	n/a	n/a	n/a	0.5	0.5	n/a	
Activation					ELU				Smax

Tabelle I: Model 1 architecture: C stands for convolutional layers and D for dense fully connected layers. ELU [32] and Smax (Softmax) are the activation functions used.

The second model has two inputs and one output. The first input is the same whitened timeseries data fed to the first model, while the second input is the Pearson correlation of each pair of detectors,

$$r_{\alpha\beta}[n] = \frac{\sum_{i=1}^N (d_\alpha[i] - \bar{d}_\alpha)(d_\beta[i+n] - \bar{d}_\beta)}{\sqrt{\sum_{j=1}^N (d_\alpha[j] - \bar{d}_\alpha)^2 \sum_{k=1}^N (d_\beta[k] - \bar{d}_\beta)^2}}. \quad (1)$$

Here  $d_\alpha[i]$  is the whitened data timeseries for detector  $\alpha$ ,  $\bar{d}_\alpha$  is the mean over  $N$  samples, and  $n$  is an integer time delay between detectors. The correlation is computed for all  $n$  corresponding to time delays of up to  $\pm 42$  ms, the largest possible light travel time between any two

points on Earth. These two inputs are fed into separate convolutional layers, termed models 2a and 2b. Finally the output of parts 2a and 2b are merged into one fully connected network which only uses dense layers. The output is a score on [0, 1], where high values indicate high correlation, as expected for a real GWB. Table II shows the architecture of this model.

Hyper Param.		Model 2a Layers								
Layer No.		1	2	3	4	5	6	7	8	9
Layer Type	C	C	C	C	C	C	C	D	D	D
Filters	32	32	32	32	32	32	32	256	256	
Kernel size	3	3	3	3	3	3	3	n/a	n/a	
Stride	2	1	2	2	2	2	2	n/a	n/a	
DropOut	n/a	n/a	n/a	n/a	n/a	n/a	n/a	0.3	0.3	
Activation								ReLU		

Hyper Param.		Model 2b Layers				
Layer No.		1	2	3	4	5
Layer Type	C	C	C	D	D	D
Filters	128	128	128	256	256	
Kernel size	3	4	4	n/a	n/a	
DropOut	n/a	n/a	n/a	0.3	0.3	
Activation				ReLU		

Hyper Param.		Model 2 merged Layers			
Layer No.		1	2	3	4
Layer Type	D	D	D	D	D
Filters	256+256	256	128	2	
DropOut	0	0.5	0	0	
Activation		ReLU		Softmax	

Tabelle II: Model 2 architecture: Model 2a and 2b both output a dense layer of size 256 with ReLU [33] activation functions. These outputs are merged and become the input of model 2c. The final output of model 2 has a Softmax activation function.

### B. Analysis Procedure

The analysis procedure is straightforward: publicly available data from the LIGO-Virgo detectors are read from files accessible from the GW open science center (GWOSC)[34] (<https://www.gw-openscience.org/O2/>). The three detectors are denoted H (Hanford), L (Livingston), and V (Virgo). The power spectral density  $S_\alpha(f)$  for each detector  $\alpha$  is computed using Welch’s method, and used to whiten the corresponding data stream. The Pearson correlation is computed between each pair of detectors. The bandpassed [20,512]Hz - whitened data series and the correlation series are then fed into the two models. Finally, the scores from the two models are multiplied together to give a combined score on [0, 1]. In this way a candidate signal needs to score highly for both models; *i.e.*, showing both coincidence in multiple detectors and correlation between the detectors.

The LIGO-Virgo data used, from GWOSC[34], were sampled at 4096 Hz. We downsample to 1024 Hz, allowing us to detect signals up to 512 Hz; this covers the most sensitive frequency range of the detectors and is sufficient for the purpose of demonstrating our CNN. (Since the trained network can process data much faster than real time, we can easily extend the analysis to higher sample rates.) We chose to focus on signal durations  $< 1$  s by analysing data in 1 s segments. This covers many plausible signal models, including for example core collapse supernovae [23], perturbed neutron stars and black holes [11], and cosmic string cusps [35]. We can easily extend to longer durations as well (with a corresponding increase in latency). At our chosen sampling rate this means that the timeseries data is fed to the CNN in an array of size [1024 x 3]. The Pearson correlation is computed for time delays in steps of one sample over  $\pm 42$  ms, for a total of 89 samples; this data is therefore in an array of size [89 x 3]. We use H as the reference and apply the time delays to the L and V timeseries.

To estimate the distribution of scores of the background noise, we repeat the analysis many times after time-shifting the data between detectors by an integer number of seconds. Since the time shift is much larger than the largest possible time-of-flight delay between detectors, it prevents a real GW signal from appearing in coincidence between multiple detectors. All coincident events in the time-shifted series can therefore be assumed to be uncorrelated and treated as background noise. This is a standard procedure in GW analysis; see *e.g.* [25].

To estimate the sensitivity to GWBs, we repeat the analysis after adding simulated signals to the data. In General Relativity, a GW has two polarisations, denoted  $h_+(t)$  and  $h_\times(t)$ . The received signal  $h_\alpha(t)$  of a given detector  $\alpha$  is the combination

$$h_\alpha(t) = F_\alpha^+ h_+(t) + F_\alpha^\times h_\times(t) \quad (2)$$

where the antenna response functions  $F_\alpha^{+,\times}$  are determined by the position and orientation of the source relative to the detector. We characterise the strength of the received signal by its network signal-to-noise ratio

$$\rho = \sqrt{\sum_\alpha 4 \int_0^\infty \frac{|\tilde{h}_\alpha(f)|^2}{S_\alpha(f)} df}. \quad (3)$$

Generating simulated signals distributed isotropically over the sky and rescaling to different  $\rho$  values allows us to measure the distribution of CNN scores as a function of the signal-to-noise ratio of the signal.

### C. Training

The choice of data used to train a CNN is a critical factor for the CNN's performance.

For the signal population we use white-noise bursts (WNBs) [25, 30]; these are signals where the  $h_+$  and

$h_\times$  polarisations are independent timeseries of Gaussian noise that is white over a specified frequency range, multiplied by a sigmoid envelope. We select these as our training sample as they are effectively featureless. The bandwidth of each injection is selected randomly and uniformly over the range [40, 480] Hz. The duration of each injection, is selected randomly and uniformly over the range [0.05, 0.9] s. The injections are distributed uniformly over the sky and projected onto the detectors using equation (2). Finally, the signal is rescaled to a desired network signal-to-noise ratio  $\rho$  as defined in equation (3).

For the background samples, we find in practice that the best CNN performance is obtained by training with *simulated* detector noise and glitches, rather than real glitchy detector noise. We therefore use Gaussian noise with a power spectrum that follows the design curve for the LIGO detectors [36] to model the stationary component of the LIGO-Virgo background noise. We model glitches by generating WNBS following the same procedure as for signals except that the WNB properties are independent and uncorrelated between detectors.

The training timeseries were constructed to emulate four different scenarios:

- **Type 1:** Gaussian LIGO-Virgo noise, with no injections. Labeled as noise.
- **Type 2:** Gaussian LIGO-Virgo noise with coherent WNB injections in all detectors, simulating a real GWB. Labeled as signal.
- **Type 3:** Gaussian LIGO-Virgo noise with different (incoherent) WNB injections in each detector, simulating unrelated glitches or excess noise in each detector. The injections may be simultaneous or offset in time from each other by up to 0.375 s to simulate simultaneous or nearly simultaneous glitches. Labeled as noise.
- **Type 4:** Gaussian LIGO-Virgo noise with a single WNB injection in a randomly chosen detector, simulating a glitch in a single detector. Labeled as noise.

We emphasise that the GWB and glitch injections were generated using the same waveform type (WNB) and drawing the signal frequency range and duration from the same distributions; our CNN is therefore forced to recognise coherence between detectors for signal/glitch discrimination rather than recognising a particular waveform morphology or time-frequency property.

All training data was generated using the MLY package [37] and its generator function, with elements of the PyCBC [38] and GWPY[39] package to project the signal onto the detectors and apply time-of-flight differences to the signals arriving at the various detector locations. For training the models we used KERAS [40]. We found empirically that training with more noise samples than signal samples helped suppress the false alarm rate of the trained models. Model 1 was trained with  $6 \times 10^4$  instances

of type 1,  $6 \times 10^4$  instances of type 2 with  $\rho$  from 12 to 40, and  $1.3 \times 10^5$  instances of type 3 with  $\rho$  from 4 to 70. Model 2 was trained with  $5 \times 10^4$  instances of type 1,  $10^5$  instances of type 2 with  $\rho$  from 10 to 50, and  $1.5 \times 10^5$  instances of type 4 with  $\rho$  from 4 to 70. Both models were trained using a learning rate of 0.002 and batch size of 30. More details and the codes are available at our repository [41].

### III. RESULTS

A standard means to assess the performance of a GWB detection algorithm (see *e.g.* [25]) is to measure the detection efficiency for various signal morphologies as a function of the signal amplitude (*e.g.*, signal-to-noise ratio) at a fixed false alarm rate.

#### A. False Alarm Rate

We calculate the false alarm rate (FAR) as a function of score by analysing background data samples that are independent from those used in the training. For this model we measured the FAR for two scenarios: for simulated Gaussian background noise (the same type of timeseries as the Type I used for training), and using real LIGO-Virgo data from the second observing run during times when all three detectors were operating (1 - 25 Aug 2017), with time shifts applied as discussed in Section II B. In each case we analysed 5184000 one-second timeseries, for a total of 60 days for each case. This choice is motivated by the **false alarm rate threshold** used by the LIGO-Virgo collaboration for issuing public alerts of candidate signals. We consider that 1 per 30 days for unmodelled searches is a good starting threshold to see if our models could be relevant for triggering electromagnetic followup observations.

The distribution of background scores is shown in Fig. 1. Gaussian noise (which has no glitches) generally gives very low scores, with a maximum measured score of approximately 0.019. Real data (which does contain glitches) produce higher scores, but even so the highest score measured over the 60 days analysed is approximately 0.43. This shows that with a sufficiently high score threshold our model is able to reject real background noise glitches even though it was trained purely on simulated data.

#### B. Detection Efficiency

We calculate the detection efficiency of our model for a selection of different possible GWB signals, both for the case of simulated Gaussian background noise and for real LIGO-Virgo data from the second observing run. In each case we generate new sets of signal injections (different from the training data) and new sets of noise

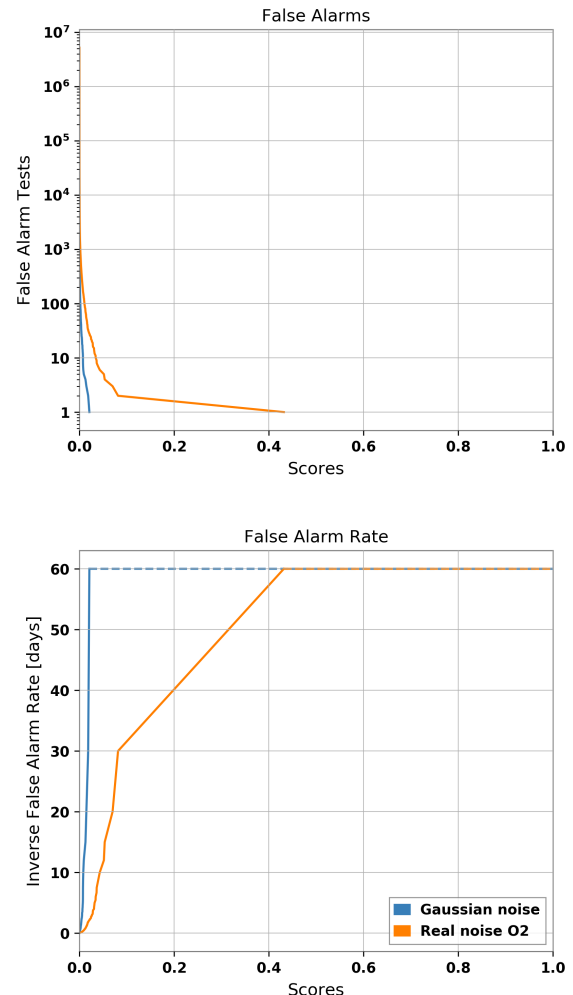


Abbildung 1: False Alarm Tests: (top) Cumulative distribution of background noise scores, for both simulated noise and real LIGO-Virgo data. Each score represents the analysis on 1s of data. (bottom) Inverse false alarm rate versus background score.

background. We measure our sensitivity to five distinct waveform morphologies:

**WNB:** These are the same type of signal as the Type II used for training.

**CSG:** A circularly polarised sinusoidal signal with Gaussian envelope. These *ad hoc* (not astrophysical) waveforms are standard for testing GWB analyses; see for example [25, 26].

**CCSN:** The N20-2 waveform of [42], from a 3D simu-

lation of a neutrino-driven core-collapse supernova (CCSN) explosion. This waveform has also been used to evaluate the sensitivity of dedicated LIGO-Virgo CCSN searches [43].

**Cusp:** The GW emission expected from cusps on cosmic strings [44]. These are also the target of dedicated LIGO-Virgo searches [45].

**BBH:** The GW signal from the inspiral, merger, and ringdown of a black-hole binary. We used the IMR-PhenomD waveform model [46][47]. The black-hole masses were selected so that all combinations of masses on  $[10, 100] M_\odot$  are utilised, the spins were randomly selected from a uniform distribution on  $[-1, 1]$ , with the restriction that the signal maximum frequency had to stay below 512 Hz.

Figure 2 shows an example waveform of each type after whitening.

Each injection timeseries is rescaled to a specific signal-to-noise ratio, added to the background timeseries, and then processed with our model. The injection is considered to be detected if the output score is larger than that of the loudest background from the FAR test (0.019 for Gaussian noise and 0.082 for real LIGO-Virgo data) at rate once per month (30 days). We tested 1000 signals of each morphology at each value of signal-to-noise  $\rho = 0, 1, 2, \dots, 50$ , where the  $\rho = 0$  case corresponds to pure noise (expected zero efficiency).

Fig.3 shows the detection efficiency for each case. We see that in simulated noise we are able to detect  $>50\%$  ( $>90\%$ ) of all signals that have amplitudes  $\rho \geq 8$  ( $\rho \geq 10$ ), with the exception of cusps for which the sensitivity is lower. The performance for CCSN and BBH signals is remarkably similar to that for WNBs, even though the signal morphologies are quite different. The performance for CSGs is even better, which we attribute to the very small time-frequency volume that it occupies. The performance for cusps is poorer, which occurs because model 1 identifies it as a glitch if it is not loud enough – an interesting demonstration of where our training could potentially be improved to handle a yet broader range of signals.

The performance in real detector data is qualitatively similar, though signals need to have  $\rho$  values approximately twice as large to be detected (detecting  $>50\%$  of all signals – excluding cusps – that have amplitudes  $\rho \gtrsim 15$ ; this is primarily due to the higher score threshold in real data for our target false alarm rate (0.082 vs. 0.019). We note that this minimal detectable  $\rho$  is already low enough to allow detection of a significant fraction of known GW events[3–7, 17], including **GW170814**[48] with IFAR  $>30$  days.

Again, the performance on CCSNe and BBHs is very similar to that for WNBs, and the performance for CSGs and cusps is again better and poorer respectively. The ability to detect CSG, CCSN, and BBH signals in real data to be particularly impressive when one considers that the CNN was not trained using any of these

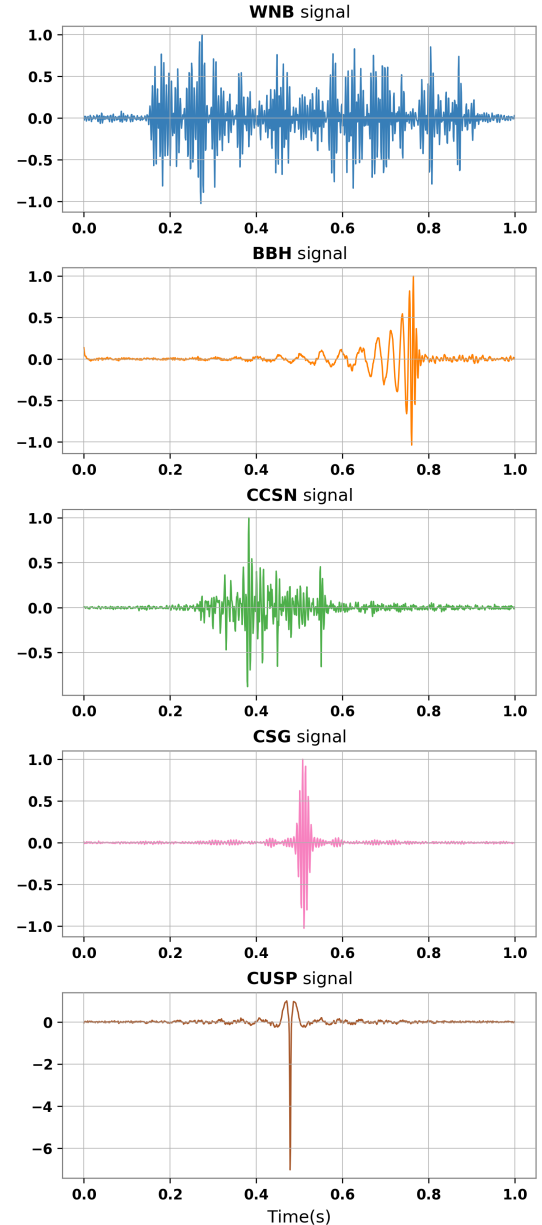


Abbildung 2: Examples of testing signals: white noise burst (WNB), binary black hole merger (BBH), core-collapse supernova (CCSN), circularly polarised sine-Gaussian (CSG) and cosmic string cusp.

data types (neither real noise nor these signal morpholo-

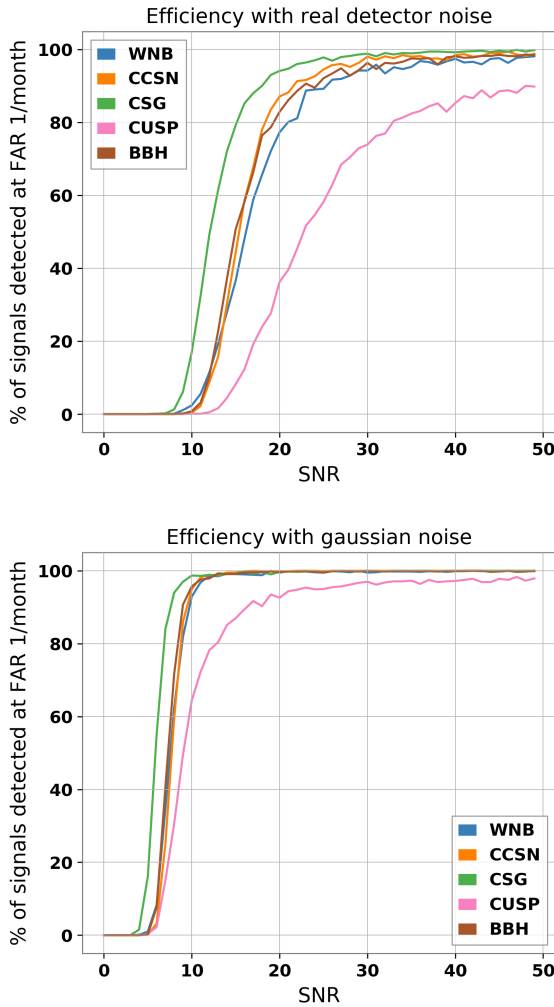


Abbildung 3: Detection efficiency tests: The fraction of simulated signals that are detected at a false alarm rate of 1 event per month versus the signal-to-noise ratio (SNR) defined by equation 3. (top) The efficiency to signals added to real detector noise, using a score threshold of 0.082. (bottom) The efficiency to signals added to simulated Gaussian noise, using a score threshold of 0.019. The waveform morphologies are white noise burst (WNB), core-collapse supernova (CCSN), circularly polarised sine-Gaussian (CSG), cosmic string cusp, and binary black hole merger (BBH).

gies). We consider this a promising demonstration of the potential of CNNs for GWB detection.

The low detection probability for signals with  $\rho \lesssim$

13 – 16 in real data partially due to the higher score threshold required for the desired false alarm rate but mainly because of the real noise being unknown to the model. This in turn is due to the small fraction of background noise samples ( $\sim 10^{-4}$ ) with scores higher than that produced by Gaussian noise. This motivates exploration of refinements to the training regimen to suppress this tail in the distribution of background scores. Moreover we note that a fraction ( $\sim 5\%$ ) of signals are missed by our algorithm even at high  $\rho$  values. This is due to cases where the two models do not agree, and merits further investigation.

We note that the CNN analysis of data is very fast: we find that the average time required to process 1 second of data, given that the data are already downloaded and available, is 51 ms on a 3.5 GHz Xeon E3-1240v5 quad-core CPU with 32 GB of RAM. This is much faster than the minute-scale latency typical of current LIGO-Virgo low-latency searches [17]. Also the time to train both models on a Tesla V100-SXM2-16GB GPU is 4 hours.

Finally, given the low latency inference of those models, we suggest that it's combination with sky-localisation pipelines [49][22] can be a complete set for an unmodelled signal search. Although we understand that this needs more work to be generalised to unmodelled signals except CBCs.

#### IV. CONCLUSIONS

We have presented a novel CNN-based analysis pipeline for the detection of transient gravitational-wave signals. Unlike previous CNN-based analyses, our pipeline is capable of detecting waveforms with morphologies that are not included in the training set while rejecting real detector noise glitches. The analysis is shown to be sensitive to a variety of waveform morphologies at signal-to-noise ratios and false alarm rates relevant for issuing rapid alerts to the astronomical community, with very low latencies and computing requirements.

Our pipeline uses a multi-component architecture where one CNN detects transients that are simultaneous in multiple detectors while a second detects correlation between the detectors to eliminate coincident background glitches. The second CNN takes as input both the whitened detector timeseries data and the Pearson correlation between detectors computed for all physically allowed light travel time delays between detectors, allowing the CNN to detect signal correlation rather than signal shape. We suggest using separate models to identify different aspects or properties of the desired signal may be a useful approach generally for GW detection with machine learning methods.

While our model already has sensitivity approaching that of standard low-latency analyses, we consider this investigation to be a promising first attempt with potential for improvement. For example, training with more sophisticated simulated and real glitches may reduce the

threshold required for the target false alarm rate, while training over a wider range of parameter space may increase sensitivity to impulsive transients similar to cosmic string cusps.

---

[1] J. A. et al., *Classical and Quantum Gravity* **32**, 074001 (2015).

[2] F. A. et al., *Classical and Quantum Gravity* **32**, 024001 (2014).

[3] B. Abbott, R. Abbott, T. Abbott, *et al.* (LIGO Scientific Collaboration and Virgo Collaboration), *Physical Review X* **9** (2019), 10.1103/physrevx.9.031040.

[4] B. P. Abbott, R. Abbott, T. D. Abbott, *et al.* (LIGO Scientific Collaboration and Virgo Collaboration), *The Astrophysical Journal* **892**, L3 (2020).

[5] R. Abbott, T. Abbott, S. Abraham, *et al.* (LIGO Scientific Collaboration and Virgo Collaboration), *Physical Review D* **102** (2020), 10.1103/physrevd.102.043015.

[6] R. Abbott, T. D. Abbott, S. Abraham, *et al.*, *The Astrophysical Journal* **896**, L44 (2020).

[7] R. Abbott, T. D. Abbott, S. Abraham, *et al.* (LIGO Scientific Collaboration and Virgo Collaboration), *Phys. Rev. Lett.* **125**, 101102 (2020).

[8] <https://gracedb.ligo.org/superevents/public/O3/>.

[9] B. P. Abbott, R. Abbott, T. D. Abbott, *et al.* (LIGO Scientific Collaboration and Virgo Collaboration), *Phys. Rev. Lett.* **116**, 061102 (2016).

[10] B. P. Abbott, R. Abbott, T. D. Abbott, *et al.* (LIGO Scientific Collaboration and Virgo Collaboration), *The Astrophysical Journal Letters* **848**:L12, 59 (2017), arXiv:1710.05833 [astro-ph.HE].

[11] K. Kyutoku, S. Fujibayashi, K. Hayashi, K. Kawaguchi, K. Kiuchi, M. Shibata, and M. Tanaka, *Astrophys. J.* **890**, L4 (2020), arXiv:2001.04474 [astro-ph.HE].

[12] B. P. Abbott, R. Abbott, T. D. Abbott, *et al.* (LIGO Scientific Collaboration and Virgo Collaboration), *Phys. Rev. Lett.* **119**, 161101 (2017).

[13] D. Kasen, B. Metzger, J. Barnes, E. Quataert, and E. Ramirez-Ruiz, *Nature* **551**, 80 (2017).

[14] B. P. Abbott, R. Abbott, T. D. Abbott, *et al.* (LIGO Scientific Collaboration and Virgo Collaboration), *Phys. Rev. Lett.* **121**, 161101 (2018).

[15] B. P. Abbott, R. Abbott, T. D. Abbott, *et al.* (LIGO Scientific Collaboration and Virgo Collaboration), *The Astrophysical Journal* **850**, L39 (2017).

[16] B. P. Abbott, R. Abbott, T. D. Abbott, *et al.* (LIGO Scientific Collaboration and Virgo Collaboration), *Nature* **551**, 85 (2017).

[17] B. P. Abbott, R. Abbott, T. D. Abbott, *et al.* (LIGO Scientific Collaboration and Virgo Collaboration), *The Astrophysical Journal* **875**, 161 (2019).

[18] D. George and E. Huerta, *Physical Review D* **97** (2018), 10.1103/physrevd.97.044039.

[19] H. Gabbard, M. Williams, F. Hayes, and C. Messenger, *Physical Review Letters* **120** (2018), 10.1103/physrevlett.120.141103.

[20] C. Bresten and J.-H. Jung, “Detection of gravitational waves using topological data analysis and convolutional neural network: An improved approach,” (2019), arXiv:1910.08245 [astro-ph.IM].

[21] H. Wang, S. Wu, Z. Cao, X. Liu, and J.-Y. Zhu, *Physical Review D* **101** (2020), 10.1103/physrevd.101.104003.

[22] C. Chatterjee, L. Wen, K. Vinsen, M. Kovalam, and A. Datta, *Physical Review D* **100** (2019), 10.1103/physrevd.100.103025.

[23] J. W. Murphy, C. D. Ott, and A. Burrows, *The Astrophysical Journal* **707**, 1173 (2009).

[24] A. L. Piro and E. Pfahl, *The Astrophysical Journal* **658**, 1173 (2007).

[25] B. P. Abbott, R. Abbott, T. D. Abbott, *et al.* (LIGO Scientific Collaboration and Virgo Collaboration), *Phys. Rev. D* **95**, 042003 (2017).

[26] B. P. Abbott, R. Abbott, T. D. Abbott, *et al.* (LIGO Scientific Collaboration and Virgo Collaboration), *Phys. Rev. D* **100**, 024017 (2019).

[27] B. P. Abbott, R. Abbott, T. D. Abbott, *et al.* (LIGO Scientific Collaboration and Virgo Collaboration), *Classical and Quantum Gravity* **33**, 134001 (2016).

[28] S. Klimenko, G. Vedovato, V. Necula, F. Salemi, M. Drago, E. Chassande-Mottin, V. Tiwari, C. Lazzaro, B. O’Brian, M. Szczepanczyk, S. Tiwari, and V. Gayathri, (2020).

[29] R. Lynch, S. Vitale, R. Essick, E. Katsavounidis, and F. Robinet, *Phys. Rev. D* **95**, 104046 (2017).

[30] P. J. Sutton, G. Jones, S. Chatterji, P. Kalmus, I. Leonor, S. Poprocki, J. Rollins, A. Searle, L. Stein, M. Tinto, and M. Was, *New Journal of Physics* **12**, 053034 (2010).

[31] N. J. Cornish and T. B. Littenberg, *Classical and Quantum Gravity* **32**, 135012 (2015).

[32] D.-A. Clevert, T. Unterthiner, and S. Hochreiter, “Fast and accurate deep network learning by exponential linear units (elus),” (2015), arXiv:1511.07289 [cs.LG].

[33] B. Xu, N. Wang, T. Chen, and M. Li, “Empirical evaluation of rectified activations in convolutional network,” (2015), arXiv:1505.00853 [cs.LG].

[34] LIGO Scientific Collaboration and Virgo Collaboration, “LIGO-Virgo strain data from observing run O2 (Nov 2016 - Aug 2017),” (2019).

[35] T. Damour and A. Vilenkin, *Phys. Rev. Lett.* **85**, 3761 (2000).

[36] B. P. Abbott, R. Abbott, T. D. Abbott, *et al.* (LIGO Scientific Collaboration and Virgo Collaboration and KAGRA Collaboration), *Living Rev Relativ* **21** (2013), arXiv:1304.0670 [gr-qc].

[37] V. Skliris, “MLy, gravitational waves and machine learning library,” <https://git.ligo.org/vasileios.skliris/mly>.

[38] A. Nitz, I. Harry, D. Brown, C. M. Biwer, J. Willis, T. D. Canton, *et al.*, “gwastro/pycbc: Pycbc release v1.16.9,” (2020).

[39] D. Macleod, A. L. Urban, S. Coughlin, T. Massinger, M. Pitkin, Rngeorge, Paulaltin, J. Areeda, L. Singer, E. Quintero, K. Leinweber, and T. G. Badger, “gwpypy/gwpypy: 2.0.1,” (2020).

[40] F. Chollet *et al.*, “Keras,” (2015).

[41] <https://git.ligo.org/vasileios.skliris/detecting-unmodeled-gravitational-wave-transients-using-convolutional-neural-networks>.

[42] Müller, E., Janka, H.-Th., and Wongwathanarat, A.,

*A&A* **537**, A63 (2012).

[43] B. P. Abbott, R. Abbott, T. D. Abbott, *et al.*, *Physical Review D* **101** (2020), 10.1103/physrevd.101.084002.

[44] T. Damour and A. Vilenkin, *Phys. Rev. D* **64**, 064008 (2001).

[45] B. P. Abbott, R. Abbott, T. D. Abbott, *et al.* (LIGO Scientific Collaboration and Virgo Collaboration), *Phys. Rev. D* **97**, 102002 (2018).

[46] S. Husa, S. Khan, M. Hannam, M. Pürrer, F. Ohme, X. J. Forteza, and A. Bohé, *Phys. Rev. D* **93**, 044006 (2016).

[47] S. Khan, S. Husa, M. Hannam, F. Ohme, M. Pürrer, X. J. Forteza, and A. Bohé, *Phys. Rev. D* **93**, 044007 (2016).

[48] B. Abbott, R. Abbott, T. Abbott, F. Acernese, K. Ackley, C. Adams, T. Adams, P. Addesso, R. Adhikari, V. Adya, and *et al.*, *Physical Review Letters* **119** (2017), 10.1103/physrevlett.119.141101.

[49] L. P. Singer and L. R. Price, *Physical Review D* **93** (2016), 10.1103/physrevd.93.024013.